

# Characteristic Analysis and Control of a Rotary Electromagnetic Eddy Current Brake

Qiao Ren, Jimin Zhang, Hechao Zhou\*, and Jinnan Luo

Institute of Railway Transit  
Tongji University, Shanghai, 201800, China  
R138150187Q@163.com, zjm2011@tongji.edu.cn, \*zhouhechao@tongji.edu.cn, tjln@tongji.edu.cn

**Abstract** — This article designs an electromagnetic rotating eddy current brake (ECB), which has the advantages of no wear and low noise compared with traditional friction brake. First, using the magnetic circuit analysis model, a theoretical calculation formula of the ECB's braking characteristics is given. The results show that the braking torque is negatively correlated with the thickness of the air gap as well as the electrical conductivity and the relative magnetic permeability of the brake disc material, and positively correlated with the number of ampere turns and the number of electromagnet poles. Secondly, a three-dimensional finite element (FE) model of the brake is established. The results of braking torque-speed characteristics between finite element calculation and theoretical analysis are compared, and the reasons for the differences between the two are explained. Using the FE model, the influence of the design parameters on torque characteristics is studied. Combined with the theoretical analysis model, the results are explained accordingly, providing a reference for the optimal design of the brake. Finally, a controller for the electromagnetic rotating eddy current brake is designed to control the amplitude of the desired braking torque.

**Index Terms** — Braking characteristics, braking torque control, eddy current brake, finite element analysis.

## I. INTRODUCTION

With the development of high-speed railways, the running speed of trains has increased significantly [1-4]. Braking systems are the guarantee of operation safety, especially for trains running at high speeds. Because the kinetic energy of high-speed trains is much larger than that of ordinary trains, both the adhesion coefficient between wheels and rails and the friction coefficient between brake shoes and moving wheels are greatly reduced at high speeds, therefore traditional mechanical braking methods cannot meet the emergency braking requirements of high-speed trains [5-7]. And friction brake has obvious defects such as fast wear and loud noise under high-speed braking conditions. The ECB is

one of the most popular braking systems because of significantly lower maintenance, no wear, and excellent braking performance at high speeds [10-11] as compared to other braking devices. The main advantage of an ECB, making it superior to the other brakes [12], is its fast dynamic response.

In this paper, an electromagnetic rotating ECB was designed, as shown in Fig. 1, mainly consisting of two parts: stator and rotor. The rotor, which is termed as the brake disc and is rotating with the axle. The stator, which is the stationary part and fixed to the train, includes several electromagnets and magnetic yokes. Each electromagnet is made up of an iron core and its surrounding coils, corresponding to the red and yellow parts in Fig. 1. When passing a certain amount of direct current (DC) into the coil, the electromagnet will generate an excitation magnetic field, meanwhile the brake disc rotating with the axle cuts magnetic induction lines in the electromagnetic field. According to the principle of electromagnetic induction, the kinetic energy of the train is converted into the eddy current in the brake disc, dissipating into the surroundings in the form of heat to achieve the purpose of braking [8-9].

Braking characteristics are defined as the variation law of braking torque with rotational speed of brake disc. While the study of braking characteristics provides the basis for making full use of ECB, current research work mostly performed their analyses of the braking characteristics of electromagnetic ECB at the theoretical and simulation level. Based on the basic macro-electromagnetic field theory, the variable separation method (VSM) was used to solve the analytical formula of braking torque [1]. In [13], a calculation method using the Laplace and Helmholtz equations was presented to analyze the eddy current generated by the transverse alternating magnetic field in two parallel conductors. In [14], Lee used the mirror image method to calculate the electric field intensity of a conductor plate with a finite radius, then introduced the magnetic flux Reynolds number to consider the armature reaction, and finally obtained a formula for calculating the braking torque through using the Lorentz formula. In [15], Liu used

the Maxwell's equations and appropriate boundary conditions to solve magnetic vector potential and magnetic flux density, and obtained their braking torque formula based on Maxwell stress tensor approach. Most recently, Reza [16] used subdomain analysis to compute the braking force for a magnetic pole moving above the induction plate.

Studies mentioned above have shown that using theoretical analysis methods to find solutions often requires a large number of premise assumptions and problem simplifications, rendering the accuracy of their results limited. For this reason, substantial efforts have been put into finite element analysis (FEA) to improve braking characteristics analysis results. For example, a 2D FE model for linear eddy current brakes was established by [17]. Compared with the simulation results, their calculation results have a higher degree of agreement in the low-speed area but greater deviation in the high-speed area. Using three-dimensional FEA, Mehmet [18] verified the effectiveness of braking torque theoretical modeling, and simulated the resistivity and permeability of the best brake disc material with finite element to obtain the maximum braking torque. Sohel [19] established a parameter model based on the FE model calculation results of braking torque characteristics, fitting the relationship between braking torque and current and speed into a polynomial function. In [20], eddy current losses of the transformer were calculated by

a 2D FE model. Their use of the Galerkin method to apply surface impedance boundary conditions to finite element calculation effectively shortened the calculation time.

As for the research on braking torque control methods, literature [21] designed a constant torque control algorithm based on the principle of controlling a constant ratio between the reference current and the speed, and verified the effectiveness of this algorithm through proportional experiments. In order to keep the braking torque constant, a dynamical compensation scheme for speed control was proposed by [22].

In this paper, an electromagnetic rotating ECB of high-speed trains is designed. We first use the magnetic equivalent circuit (MEC) to study the dynamic characteristics of the ECB system, and offer a brief mathematical model of the braking characteristics to clarify the main parametric factors that affect the braking torque. Secondly, a three-dimensional FE model of the brake is established to specifically quantify the influence of each parameter factor on the braking characteristics. Then the differences between the braking torque-speed-current characteristics curve calculated by the theoretical model and the FE model are compared and analyzed to offer sensible explanations. Finally, a fuzzy controller for the electromagnetic rotating ECB is designed to accurately track the desired braking torque.

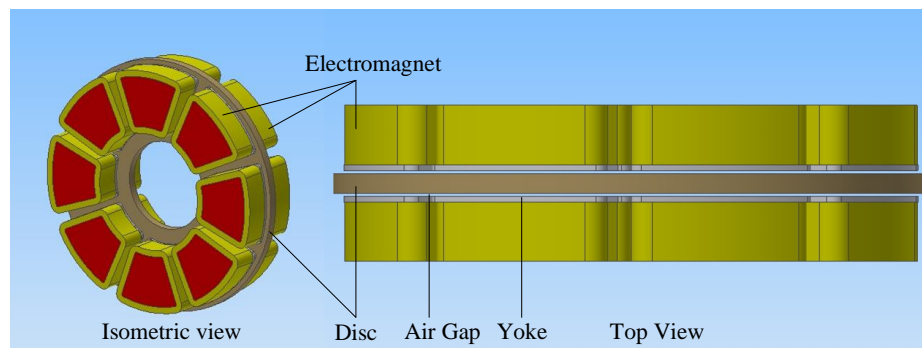


Fig. 1. Configuration of the eddy current brake.

## II. ANALYTICAL MODEL

This article derives the brake disc eddy current, air gap magnetic field and eddy current power according to the differential principle. Starting from the law of energy conservation, the eddy current power is regarded equal to braking power, and the braking torque is obtained according to the relationship between power and torque.

### A. Model assumptions

To facilitate the derivation of braking torque, the following assumptions are made for the model:

(1) The influence of temperature on the electromagnetic properties are neglected.

(2) The magnetic flux lines are ideally distributed only within the projection areas on the disc of yokes.

(3) The magnetic saturation and nonlinearity of magnetic properties are neglected.

### B. Eddy current analysis

The projection area of a single yoke on the brake disc is a sector, as shown in Fig. 2, whose inner and outer radii are  $r_1$  and  $r_2$ , respectively, with a  $40^\circ$  angle. From the perspective of differentiation principle, this sector is regarded as composed of countless similar sector-shaped rings (shadowed) with a width of  $dr$ , and the position of these sector-shaped rings can be represented by the

distance  $r$  from the inner and outer arcs to the middle radius of the large sector, where  $r \in [0, \Delta r]$ ,  $\Delta r = r_c - r_1 = (r_2 - r_1)/2$ ,  $r_c = (r_1 + r_2)/2$ .

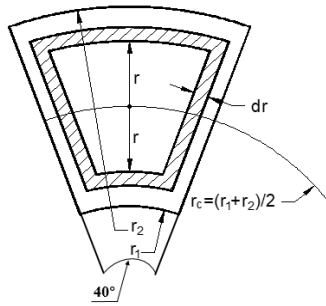


Fig. 2. Projection area of a single yoke on the brake disc.

The magnetic flux passing through the sector area can be expressed as:

$$\phi_r = BS_r \cos \omega_n t = \frac{4\pi r_c r B \cos \omega_n t}{9}, \quad (1)$$

where,  $S_r$  is the area of the inner sector surrounded by the sector ring, which can be calculated according to Eq. (2) below.  $B$  is the magnetic induction density value on the surface of the brake disc, and  $\omega_n$  is the electrical angular velocity of the brake disc:

$$S_r = \frac{40^\circ}{360^\circ} \times \pi[(r_c + r)^2 - (r_c - r)^2] = \frac{4\pi r_c r}{9}, \quad (2)$$

$$\omega_n = N_p \cdot \omega = N_p \cdot \frac{2\pi n}{60} = \frac{\pi N_p n}{30}, \quad (3)$$

where  $N_p$  is the number of pole pairs on one side of the disc,  $\omega$  is the angular velocity of the disc, and  $n$  is the rotation speed of the disc.

The induced electromotive force is:

$$\varepsilon_r = -\frac{d\phi_r}{dt} = \frac{4\pi r_c r B \omega_n \sin \omega_n t}{9}. \quad (4)$$

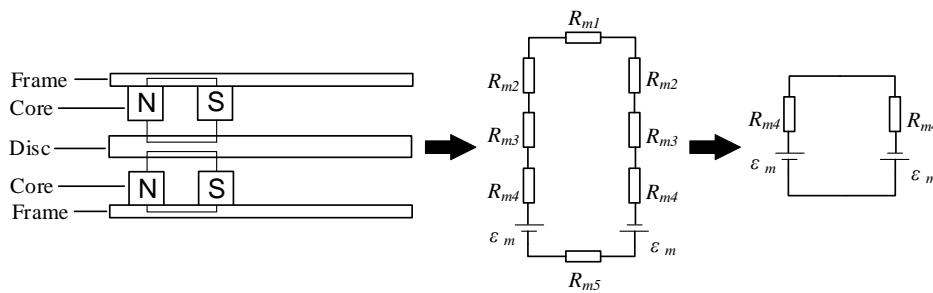


Fig. 3. Magnetic circuits.

According to Fig. 3, the magnetic circuit can be written as:

$$\varepsilon_m = R_{m4} \cdot \phi, \quad (9)$$

where the magnetoresistance of the air gap is:

The resistance of the sector ring is:

$$R_r = \rho \frac{L_r}{d' \cdot dr}, \quad (5)$$

where,  $d'$  and  $L_r$  are the skin depth of the vortex and the length of the sector ring, respectively. And  $d'$  satisfies the following formula:

$$d' = \sqrt{\frac{2\rho}{\mu_0 \mu_r \omega_n}}, \quad (6)$$

where,  $\rho$  is the resistivity of the brake disc,  $\mu_0$  is the vacuum permeability,  $\mu_r$  is the relative permeability of the brake disc.

Thus, according to the Ohm's law, the current value on the sector ring, that is, the eddy current value can be expressed as:

$$i_r = \frac{\varepsilon_r}{R_r} = \frac{\sqrt{2} r_c r B \omega_n \sin \omega_n t dr}{(r + \pi r_c) \sqrt{\rho \mu_0 \mu_r \omega_n}}. \quad (7)$$

### C. Magnetic field analysis

The Ohm's law for a magnetic circuit can be derived from Maxwell equations:

$$\varepsilon_m = \sum R_{mi} \cdot \phi_i, \quad (8)$$

where  $\varepsilon_m$  is the magnetomotive force,  $\phi$  is the magnetic flux,  $\phi = BS_p$ ,  $S_p$  is the area of the total sector shown in Fig. 2,  $R_{mi}$  represents every magnetic resistance in the magnetic circuit.

The simplified magnetic circuit and the definition of each part reluctances are shown in Fig. 3.  $R_{m1}$ ,  $R_{m2}$ ,  $R_{m3}$ ,  $R_{m4}$ ,  $R_{m5}$  are the magnetic resistances of the frame, core, yoke, air gap, and disc, respectively. Since the relative permeability of the frame, core and disc is much higher than that of air which approximately equals 1, only  $R_{m4}$  is taken into consideration in this paper.

$$R_{m4} = \frac{\delta}{\mu_0 \mu_{r4} S_p} \approx \frac{\delta}{\mu_0 S_p}, \quad (10)$$

where,  $\delta$  and  $\mu_{r4}$  are the length of air gap and air relative permeability, respectively.

The total magnetic motive force  $\varepsilon_m$  is given as:

$$\varepsilon_m = \varepsilon_0 - \varepsilon_e, \quad (11)$$

where  $\varepsilon_0$  and  $\varepsilon_e$  are the magnetic motive forces generated by electromagnets and eddy current, respectively, and they are given as:

$$\varepsilon_0 = NI, \quad (12)$$

$$\varepsilon_e = k_e \cdot I_e, \quad (13)$$

where  $N$  is the number of turns per coil,  $I$  is the excitation current,  $k_e$  is the computation coefficient,  $I_e$  is the RMS eddy current which can be obtained by integration of the eddy current  $i_r$ :

$$I_e = \frac{1}{\sqrt{2}} \int_0^{\Delta r} i_r = \frac{r_c B \omega_n}{\sqrt{\rho \mu_0 \mu_r \omega_n}} \cdot (\Delta r - \pi r_c \ln \frac{\Delta r + \pi r_c}{\pi r_c}). \quad (14)$$

From Eqs. (9)-(14), we can derive that the magnetic flux density is:

$$B = \frac{\mu_0 NI \sqrt{\rho \mu_0 \mu_r}}{\delta \sqrt{\rho \mu_0 \mu_r} + k_e r_c \mu_0 \sqrt{\omega_n} (\Delta r - \pi r_c \ln \frac{\Delta r + \pi r_c}{\pi r_c})}. \quad (15)$$

#### D. Power analysis

The RMS power of eddy current of the whole disc  $P_e$  can be obtained by integration of the product of eddy current  $i_r$  and the induced electromotive force  $\varepsilon_r$ :

$$\begin{aligned} P_e &= 2 \times \frac{360^\circ}{40^\circ} \times \frac{1}{\sqrt{2}} \int_0^{\Delta r} i_r \cdot \varepsilon_r \\ &= \frac{4\sqrt{2}\pi r_c^2 B^2 \omega_n^2}{\sqrt{\rho \mu_0 \mu_r \omega_n}} \cdot \left[ \frac{1}{2} \Delta r^2 - \pi r_c \Delta r \right. \\ &\quad \left. + (\pi r_c)^2 \cdot \ln \frac{\Delta r + \pi r_c}{\pi r_c} \right]. \end{aligned} \quad (16)$$

#### E. Torque analysis

The brake power  $P_b$  equals the RMS power of eddy current  $P_e$  in accordance with the law of conservation of energy, therefore the following expression can be obtained:

$$P_b = P_e = T_b \cdot \omega, \quad (17)$$

where  $T_b$  is the torque generated by the eddy current brake. From (16)-(17) and the relation between the angular velocity  $\omega$  and the train speed  $v$ , we can derive that the brake torque is:

$$T = \frac{4\sqrt{10}\pi k_1 r_c^2 \mu_0^{\frac{5}{2}} (\mu_r \rho)^{\frac{1}{2}} (NI)^2 N_p^{\frac{3}{2}} D_w^{-\frac{1}{2}} v^{\frac{1}{2}}}{3(\delta \sqrt{\rho \mu_0 \mu_r} + k_2 k_e r_c \mu_0 \sqrt{\frac{5N_p v}{9D_w}})^2}, \quad (18)$$

where  $k_1, k_2$  are both coefficients that are determined by the geometric parameters of the brake device,  $D_w$  is the diameter of the wheel.

### III. VALIDATION OF THE FE MODEL

Brake torque is influenced by the geometric and electromagnetic parameters according to the above theoretical model. More specifically, there is a negative correlation between brake torque and the length of air gap, the inner radius of yoke, the product of the resistivity and permeability of disc material, and a positive correlation between brake torque and the number of poles, the outer radius of yoke. In addition, brake torque is proportional to the square of ampere turns of electromagnets. In order to analyze the quantitative effects of each factor on the braking performance and verify the accuracy of the analytical model, a 3D FE model was established for further numerical calculations, as shown in Fig. 4. Only the brake disc, yokes, and electromagnets were considered in the FE model because of the assumption that the other components only act as fixed support and no magnetic lines pass through them. So, their effects on the magnetic field can be ignored. In the FE model, the material of electromagnet core and brake disc is mild steel steel\_1008. The material of magnetic yoke is mild steel steel\_1010, and the material of electromagnet coil is copper. A 1/4Np simplified model is adopted to reduce simulation time. For this reason, a symmetry boundary condition is added in the middle section of the brake disc. Master and slave boundary conditions are implemented in the two sides considering the electromagnets' periodic distribution. Main parameters of the FE model are given in Table 1.

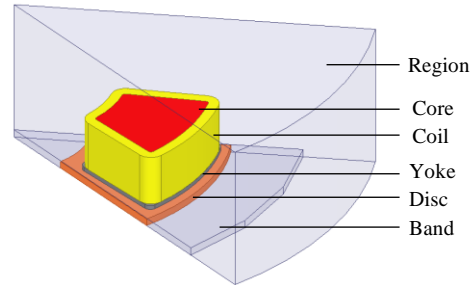


Fig. 4. FE model.

The magnetic flux density map, eddy current losses and the distribution of induced eddy currents are shown in Figs. 5 (a), (b) and (c) respectively. It can be seen that 2.2T magnetic flux density is obtained by the FE model. And at the same parameters, the air gap magnetic flux density of 2.34T is calculated based on the analytical model. The value of relative error is about 6.3%. Hence, the results of the analytical model are in good agreement with the FE model results. In addition, eddy current losses are calculated by the FE model and Eq. (16), as shown in Fig. 6. It can be seen that both the analytical model and FE model have the same linear growth trend. The eddy current losses increase with the speed increases.

Table 1: ECB Parameters

| Parameter   | Value |
|---|-------|
| Inner radius of the disc                            | 210mm |
| Outer radius of the disc                            | 600mm |
| Disc thickness                                      | 20mm  |
| Air gap width                                       | 3mm   |
| Inner radius of the yoke                            | 280mm |
| Outer radius of the yoke                            | 580mm |
| Yoke thickness                                      | 6mm   |
| Core thickness                                      | 60mm  |
| Angle covered by a single electromagnet             | 40deg |
| Angle between two adjacent electromagnets           | 45deg |
| Number of pole pairs on one single side of the disc | 4     |
| Number of turns per coil                            | 400   |
| Excitation current                                  | 40A   |

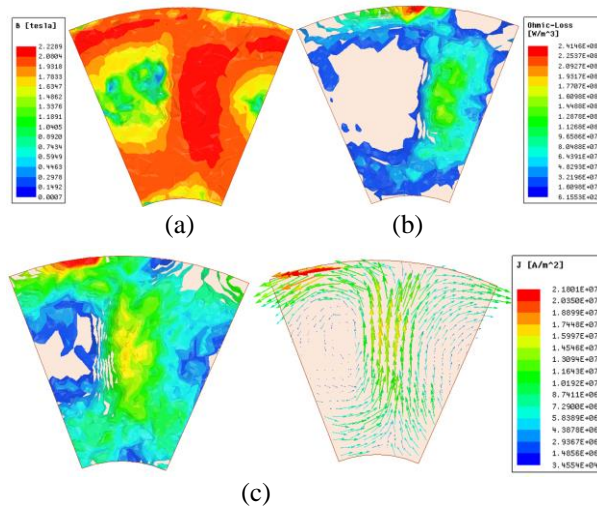


Fig. 5. (a) The magnetic flux density map, (b) eddy current loss, and (c) distribution of induced eddy currents.

At the initial simulation time, a large amplitude fluctuation of the braking torque appeared and then converged to a steady value. This phenomenon is inevitable due to the initial value of calculation changes to the target value suddenly. It was only regarded steady-state values as the effective data and calculated the final torque-speed characteristic curve. Figure 7 shows a comparison between the FE model and analytical model of braking torque-speed characteristics. It is observed that the braking characteristics tendency of the analytical model is consistent with that of the FE model. Still, the results from analytical method in Eq. (18) are slightly larger than those from FE at the whole speed range. When the vehicle speed is higher than the critical speed, the decrease of braking torque calculated by FE is more evident than that calculated by Eq. (18). This is due to

the assumptions made to simplify the theoretical analysis, especially assumption (3), in which we assumed that the magnetic saturation and nonlinearity of magnetic properties are neglected. Additionally, in the analytical model, the effects of flux leakage and uneven distribution of magnetic field lines are ignored, which also cause the theoretical value to be too large.

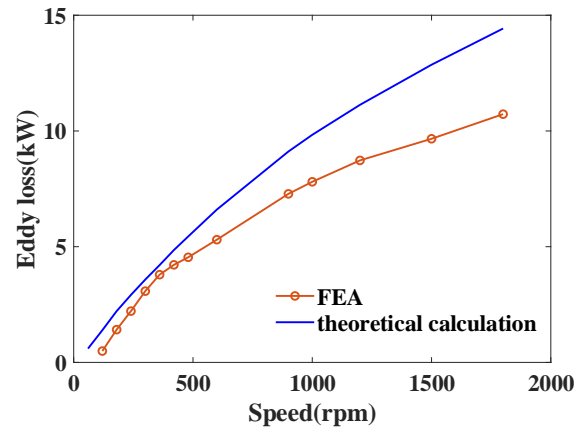


Fig. 6. Eddy current losses.

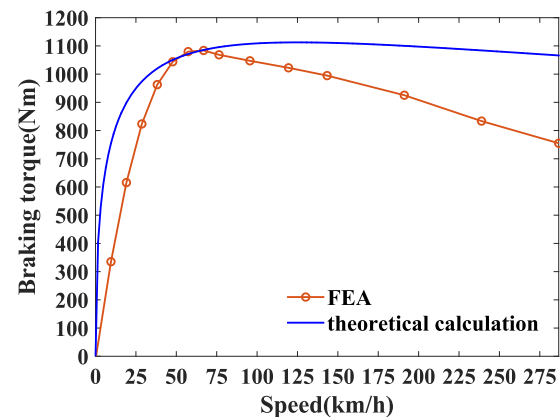


Fig. 7. Braking torque-speed characteristic.

#### IV. PARAMETER ANALYSIS

It is found by FEA that the excitation current, air gap thickness, brake disc thickness and electromagnet core shape have more significant influence on the braking characteristic, so the influence of these four factors on braking characteristics is specifically analyzed in this paper.

##### A. Influence of the excitation current

Figure 8 shows the variation of braking torque characteristics for  $I=40,60,80,100A$  while keeping other parameters unchanged. It is obvious that the braking torque increases gradually as the excitation current increases. And the peak torque increases in a trend of

linear function. However, from Eq. (18), the braking torque should be proportional to the square of the excitation current. The main reason for this difference is that electromagnets have nonlinear magnetization characteristics. The magnetic permeability decreases as the excitation current increases so that the magnetic induction intensity shows a nonlinear growth trend with a declining growth rate. Furthermore, the critical speed increases with the increase of excitation current. According to Eq. (6), the skin depth increases as the magnetic permeability decreases, which weakens the eddy current skin effect. Therefore, if the eddy current magnetic field is to reach its original strength, it needs to increase the speed [17].

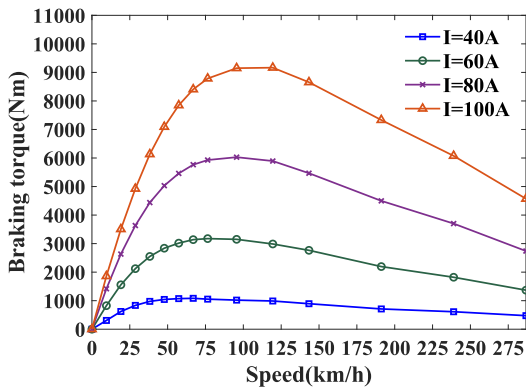


Fig. 8. Braking torque-speed characteristics for different excitation currents.

**B. Influence of the air gap length**

Figure 9 shows the variation of braking torque characteristics for air gap=3,4,5,6mm, while other parameters are kept to values introduced earlier. It is observed that a shorter air gap length leads to higher braking torque values. This is due to a large air gap length will result in a larger magnetoresistance, which will cause a lower magnetic density. In addition, for a large air gap, the torque-speed characteristic curves of the high-speed region are flatter than that of a small air gap. This is due to the former's eddy current being far away from the yoke compared to the latter, which causes a lesser demagnetization effect on the original magnetic field.

**C. Influence of the conductor plate thickness**

The effect of the conductor plate thickness on the braking torque-speed characteristic has been studied by changing the thickness from 15 to 30 mm in a step of 5mm. From Fig. 10, the thinner the conductor plate is, the higher the peak torque and the critical speed would be for the ECB. The reason is that eddy currents in the conductor plate increase as the thickness of the conductor plate increases, which intensifies the influence

of the eddy current magnetic field on the excitation magnetic field. Therefore, the braking torque reaches the peak value at a low speed, and the peak torque becomes small due to the eddy current demagnetization effect.

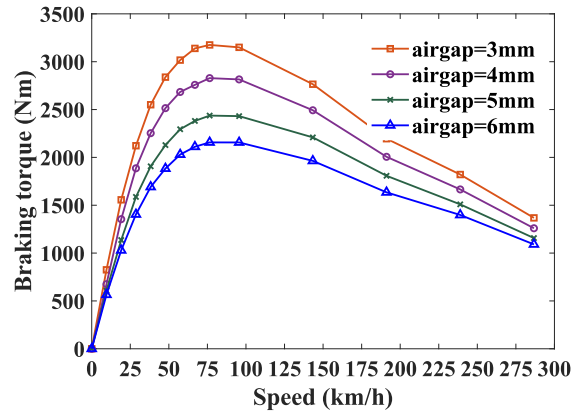


Fig. 9. Braking torque-speed characteristics for different air gap lengths.

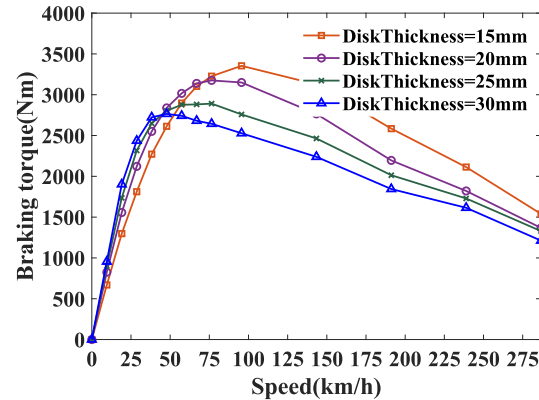


Fig. 10. Braking torque-speed characteristics for different disc thicknesses.

**D. Influence of the pole shape**

The electromagnet core is designed to be round, square, and sector in turn while keeping the cross-sectional area of the electromagnet core unchanged. The torque-speed characteristics for three kinds of electromagnet core shapes are shown in Fig. 11. We can observe that an optimum torque generation capacity exists for the sector-shaped section electromagnet. Because of the fact that only the tangential electromagnetic force generated by the radial eddy current can contribute to the braking torque. In contrast, the tangential eddy current is ineffective for braking torque generation. Electromagnets with circular and square cross-sections have a lesser radial coverage of the projection area on the brake disc than sector-shaped section electromagnets, resulting in a small effective

braking torque. In order to enlarge the path of the radial eddy current, a sector-shaped section electromagnet is designed. The adequate electromagnetic torque can be enhanced by increasing the eddy current flowing along the radius of the disc with the sector pole [18].

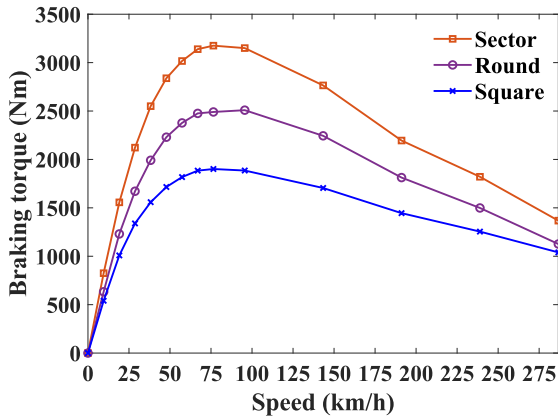


Fig. 11. Braking torque-speed characteristics for different pole shapes.

## V. EDDY CURRENT BRAKE CONTROL SYSTEM

### A. Braking torque controller design

Based on the above theoretical calculation of braking torque and the FEA of braking characteristics, the braking torque decreases with the increase of speed in the high-speed region. In order to track the desired braking torque accurately, this paper presents a controller based on the fuzzy method to control the amplitude of the braking torque. Figure 12 shows the control scheme of the ECB. It consists of a braking torque controller and a current controller. The braking torque controller outputs the reference of the excitation current change  $\Delta I_{ref}$  according to the error between the desired braking torque  $T_{ref}$  and the actual braking torque  $T_b$ . The current controller is composed of a current hysteresis controller and a DC chopper circuit, which outputs a reference voltage  $u_{ref}$  according to the reference value of the excitation current change. One can adjust the excitation current to regulate the value of the braking torque by controlling the reference voltage.

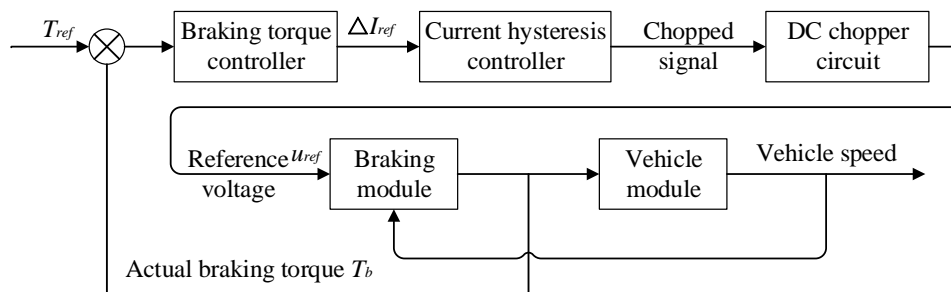


Fig. 12. The overall scheme of the torque control system.

### B. Control algorithm description

In the fuzzy controller, the system input variables are the braking torque error  $e$  and its rate of change  $ec$ . The output variable is the change of reference current  $\Delta I_{ref}$ . Design variables use the same set of fuzzy state words {NB, NS, PS, PB}, in which each fuzzy state corresponds to {‘negative big’, ‘negative small’, ‘positive small’, ‘positive big’}, denoting the variables sign and absolute value size. The membership function for the fuzzy sets is set as a triangular function, as shown in Fig. 13. According to the qualitative relationship between the braking torque error and the change of reference current, the fuzzy rule table is formulated as shown in Table 2. The center of gravity method, the most commonly used defuzzification method, is used in this paper.

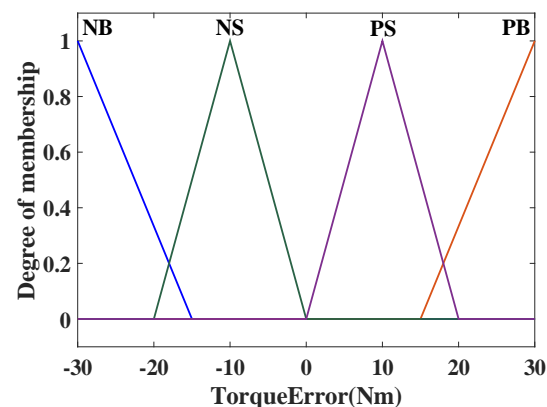


Fig. 13 Membership function for fuzzy sets.

Table 2: Fuzzy rules

| Error $e$ | Change of $ec$ |    |    |    |
|-----------|----------------|----|----|----|
|           | NB             | NS | PS | PB |
| NB        | NB             | NB | NB | NB |
| NS        | NB             | NS | NS | NS |
| PS        | NS             | PS | PS | PB |
| PB        | PB             | PB | PB | PB |

## VI. ANALYSIS OF THE SIMULATION RESULTS

In Fig. 14, the variation of the braking torque is plotted with respect to varying speeds of the rotating disk under open-loop control and closed-loop control algorithms. In this paper, PID control and fuzzy control are carried out. It is evident that the braking torque increases firstly and then decreases as the speed increases under open-loop control, which causes the fluctuation of the train braking deceleration. Note that the braking torque keeps constant as the speed varies under closed-loop control. This is because the control system adjusts the excitation current in real-time according to the braking torque feedback. In the speed range of 20-160  $km/h$ , the actual braking torque is controlled near the desired braking torque. As the speed continues to decrease, the maximum braking torque output is limited by the coil current in the low-speed region, the braking torque starts to drop. It can be concluded that the two control algorithms mentioned can effectively control the braking torque to remain constant in an extensive speed range.

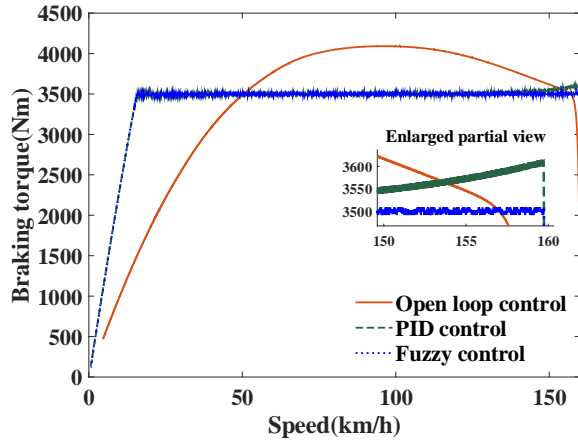


Fig. 14. Brake torque versus train speed under different control algorithms.

In Fig. 15, the time response curve of the braking torque is shown. In order to quantitatively illustrate the control effect of the two algorithms, the transient and steady-state performance indicators of the system are calculated in Table 3. It can be seen that from transient

performance indicators, the maximum overshoot of the system under PID control is 111.7N·m, which is far greater than the overshoot of 26.2N·m under fuzzy control. In addition, the adjustment time of the system under PID control is 3.210s, which is longer than 0.318s under fuzzy control. In terms of steady-state performance indicators, the steady-state value of the system under the fuzzy control is closest to the desired braking torque of 3500N·m. However, the result under the PID control deviates from the expected value significantly. It can be concluded that fuzzy control is better than PID control in both transient and steady-state indicators.

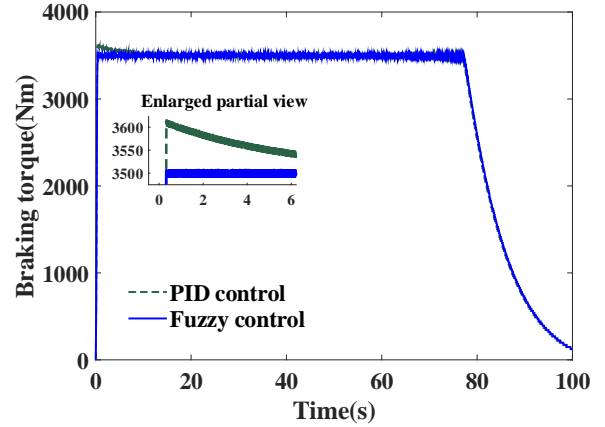


Fig. 15. Brake torque under different control algorithms.

Table 3: System performance indicators

|                        | Performance                     | PID    | Fuzzy Control |
|------------------------|---------------------------------|--------|---------------|
| Transient indicator    | Adjustment time $t_s/(s)$       | 3.210  | 0.318         |
|                        | Peak time $t_p/(s)$             | 0.333  | 0.323         |
|                        | Maximum overshoot $\sigma/(Nm)$ | 111.7  | 26.2          |
| Steady-state indicator | Steady state average $/(Nm)$    | 3502.3 | 3499.3        |
|                        | Steady state maximum $/(Nm)$    | 3524.4 | 3504.6        |
|                        | Steady state minimum $/(Nm)$    | 3489.1 | 3497.3        |

## VII. CONCLUSIONS

In this paper, an electromagnetic rotating eddy current brake is regarded as the research object. Studying the braking characteristic from two aspects of theoretical analysis and FEA, and designing a braking torque controller. The main conclusions can be drawn as follows:

- (1) The theoretical model shows that the braking

torque is negatively correlated to the air gap length, the electrical conductivity and relative permeability of the brake disc material, and positively correlated to the number of ampere turns and the number of pole pairs.

(2) There are differences between the results of FEA and theoretical analysis. The main reason for the difference is that the theoretical model neglects nonlinear characteristics of the brake disc material, the magnetic saturation phenomenon of electromagnets, and the non-ideal distribution of the magnetic flux.

(3) The relationship between the braking torque and the design parameters such as excitation current, air gap length, brake disc thickness, and electromagnet shape on the braking characteristics is analyzed using the FEA, which provides a reference for the optimal design of the ECB.

(4) An ECB controller based on fuzzy control theory is designed. Compared with open-loop control and PID control, the proposed controller can keep the braking force stable during the train braking process.

#### ACKNOWLEDGMENT

This work was supported by the Shanghai Collaborative Innovation Center for Multi-network and Multi-mode Rail Transit under Grant 28002360012.

#### REFERENCES

- [1] X. Zhu and X. Zhang, "Analysis and calculation of braking force on rail eddy current braking of high speed trains," [J]. *Journal of Tongji University (Natural Science)*, vol. 17, no. 4, pp. 1-8, Dec. 1996.
- [2] C. Yin and K. Zhang, "Electromagnetic force calculation of conductor plate double Halbach permanent magnet electrodynamic suspension," *Applied Computational Electromagnetics Society Journal*, vol. 29, no. 11, pp. 916-922, Nov. 2014.
- [3] M. Fujita, T. Tokumasu, T. Yamada, T. Hirose, Y. Tanaka, N. Kumagai, and S. Uchida, "3-dimensional electromagnetic analysis and design of an eddy-current rail brake system," *IEEE Transactions on Magnetics*, vol. 34, no. 5, pp. 3548-3551, Sept. 1998.
- [4] S. Surenkhorloo and J. K. Byun, "Analysis and case study of permanent magnet arrays for eddy current brake systems with a new performance index," *Journal of Magnetics*, vol. 18, no. 3, pp. 276-282, Sept. 2013.
- [5] C. Aldo and B. Vusini, "Design of axial eddy-current couplers," *IEEE Transactions on Industry Applications*, vol. 39, no. 3, pp. 725-733, May 2003.
- [6] L. Thierry and A. Rezzoug, "3-D analytical model for axial-flux eddy-current couplings and brakes under steady-state conditions," *IEEE Transactions on Magnetics*, vol. 51, no. 10, pp. 1-12, July 2015.
- [7] Z. Ali and A. Mirabadi, "Railway wheel detector in the presence of eddy current brakes," *Applied Computational Electromagnetics Society Journal*, vol. 28, no. 1, pp. 77-84, Jan. 2013.
- [8] B. Kou, Y. Jin, H. Zhang, L. Zhang, and H. Zhang, "Analysis and design of hybrid excitation linear eddy current brake," *IEEE Transactions on Energy Conversion*, vol. 29, no. 2, pp. 496-506, Mar. 2014.
- [9] K. Kerem, A. Suleman, and E. J. Park, "Analytical modeling of eddy current brakes with the application of time varying magnetic fields," *Applied Mathematical Modelling*, vol. 40, no. 2, pp. 1168-1179, Jan. 2016.
- [10] J. R. Tibola, R. L. Sari, T. D. M. Lanzasova, M. E. S. Martins, and H. Pinheiro, "Modeling and control of a low-cost driver for an eddy current dynamometer," *Journal of Control, Automation and Electrical Systems*, vol. 27, no. 4, pp. 368-378, Apr. 2016.
- [11] B. Kou, Y. Jin, L. Zhang, and H. Zhang, "Characteristic analysis and control of a hybrid excitation linear eddy current brake," *Energies*, vol. 8, no. 7, pp. 7441-7464, July 2015.
- [12] C. Tian, M. Wu, L. Zhu, and J. Qian, "An intelligent method for controlling the ECP braking system of a heavy-haul train," *Transportation Safety and Environment*, vol. 2, no. 2, pp. 133-147, June 2020.
- [13] T. Szczegielniak, P. Jabłoński, D. Kusiak, and Z. Piątek, "Eddy currents induced in two parallel round conductors," *Applied Computational Electromagnetics Society Journal*, vol. 34, no. 12, pp. 1922-1930, Dec. 2019.
- [14] L. Kapjin and K. Park, "Modeling eddy currents with boundary conditions by using Coulomb's law and the method of images," *IEEE Transactions on Magnetics*, vol. 38, no. 2, pp. 1333-1340, Aug. 2002.
- [15] Y. Reza and M. Mirsalim, "Axial-flux wound-excitation eddy-current brakes: Analytical study and parametric modeling," *IEEE Transactions on Magnetics*, vol. 50, no. 6, pp. 1-10, Jan. 2014.
- [16] Z. J. Liu, A. Vourdas, and K. J. Binns, "Magnetic field and eddy current losses in linear and rotating permanent magnet machines with a large number of poles," *IEE Proceedings A-Science, Measurement and Technology*, vol. 138, no. 6, pp. 289-294, Dec. 1991.
- [17] M. Hecquet, P. Brochet, L. Jin, and P. Delsalle, "A linear eddy current braking system defined by finite element method," *IEEE Transactions on Magnetics*, vol. 35, no. 3, pp. 1841-1844, May 1999.
- [18] G. Mehmet, E. Yolacan, and M. Aydin, "Design, analysis and real time dynamic torque control of single-rotor-single-stator axial flux eddy current

brake,” *IET Electric Power Applications*, vol. 10, no. 9, pp. 869-876, Nov. 2016.

- [19] A. Sohel, “A parametric model of an eddy current electric machine for automotive braking applications,” *IEEE Transactions on Control Systems Technology*, vol. 12, no. 3, pp. 422-427, May 2004.
- [20] J. M. Díaz-Chacón, C. Hernandez, and M. A. Arjona, “A comprehensive 2D FE-SIBC model for calculating the eddy current losses in a transformer tank-wall,” *Applied Computational Electromagnetics Society Journal*, vol. 27, no. 8, pp. 646-653, Aug. 2012.
- [21] H. J. Ryoo, J. S. Kim, D. H. Kang, G. H. Rim, Y. J. Kim, and C. Y. Won, “Design and analysis of an eddy current brake for a high-speed railway train with constant torque control,” *Conference Record of the 2000 IEEE Industry Applications Conference*, Rome, Italy, vol. 1, pp. 277-281, Oct. 2000.
- [22] S. Emmanuel and D. Georges, “Modeling and control of eddy current brake,” *IFAC Proceedings Volumes*, vol. 28, no. 8, pp. 109-114, July 1995.



levitation control.

**Qiao Ren** graduated from Changan University in 2018 with a bachelor's degree. She is currently working toward the Ph.D. degree with the Institute of Railway Transit, Tongji University, China. Her current research interests include eddy current brake, high-speed magnetic



electromechanical coupling and active vehicle safety control, etc.

**Jimin Zhang** received his M.Sc. and Ph.D. degrees from Southwest Jiaotong University, Chengdu, China, in 1999, and 2004, respectively. Since 2004, he has been with Tongji University, where he is currently a Professor. His research interests include magnetic levitation control,



high-speed magnetic levitation and vehicle system dynamics, etc.

**Hechao Zhou** received his M.Sc. and Ph.D. degrees from Tongji University and Technische Universität Berlin, in 2010, and 2014, respectively. Since 2014, he has been with Tongji University, where he is currently an Assistant Professor. His research interests include high-



**Jinnan Luo** received his B.S. degree in 2018 and M.Sc. degree in 2021 from Tongji University, Shanghai, China. His interest is high-speed magnetic field analysis and eddy current brake.